

Numerical solution for the stress near a hole with corners in an infinite plate under biaxial loading

Weiqi Wang · Brian J. Spencer

Received: date / Accepted: date

Abstract We consider the elastic stress near a hole with corners in an infinite plate under biaxial stress. The elasticity problem is formulated using complex Goursat functions, resulting in a set of singular integro-differential equations on the boundary. The resulting boundary integral equations are solved numerically using a Chebyshev collocation method which is augmented by a fractional power term, derived by asymptotic analysis of the corner region, to resolve stress singularities at corners of the hole. We apply our numerical method to the test case of the hole formed by two partially-overlapping circles, which can include either a corner pointing into the solid or a corner pointing out of the solid. Our numerical results recover the exact stress on the boundary to within relative error 10^{-3} for modest computational effort.

Keywords elasticity · Goursat functions · boundary integral equations · numerical methods · corners · stress singularities

1 Introduction

Free boundary elasticity problems are fundamental to describing crystal growth in strained solids. Due to the slow time scale of crystal growth relative to the time scale of elastic relaxation, the elastic response can be described by the quasi-static elasticity problem: a time-dependent free or moving boundary problem for the morphology of the solid surface coupled to the static elasticity equations in the solid. Thus, efficient

This work was supported by a grant from the Simons Foundation (Award #354717, BJS).

Weiqi Wang
Department of Mathematics, University at Buffalo, Buffalo, NY 14260, USA
Tel.: +(716)-352-3644
E-mail: weiqiwan@buffalo.edu

Brian J. Spencer
Department of Mathematics, University at Buffalo, Buffalo, NY 14260, USA
Tel.: +(716)-645-8805
E-mail: spencerb@buffalo.edu

computational methods for solving the static elasticity problem for general boundary shapes are necessary.

The formulation of the elasticity problem for a given system with a free or moving boundary can correspond to an interior domain, an exterior domain, or a semi-infinite domain with boundaries that are smooth or allowed to have corners. More complicated systems can have multiple domains of elastically-interacting solid phases. Our focus here is on the fundamental geometry of a hole (or void) inside a two-dimensional elastically-stressed solid, for the case when the domain has corners and the stress field has singularities at the corner.

There are of course exact solutions for the stressed infinite plate with holes of different geometries. But many of these results apply only to pre-defined hole geometries without corners (e.g. a circle [21] or ellipse [17]), or for pre-defined geometries in which there is some imposed geometric rounding of the corner (eg. a rectangle with rounded corners [24, 22, 20]), or in special hole-with-corner configurations (e.g. a hole formed by partially overlapping circles [18]). But all of these results are for holes of fixed geometry and thus require the hole shape to be known in advance and are not useful for solving a free boundary problem. In principle, the elasticity solution for an arbitrarily shaped hole can be determined by using a conformal map of the hole boundary to a circle (e.g. Schwarz–Christoffel mapping [8]), but in most cases the conformal map approach will not work if the original domain has a corner.

One approach to the problem of finding the solution for a domain with corners is to impose some mechanism for rounding the corner which gives a smooth boundary for the hole from which the elasticity solution can be found. For example, the rectangular-hole solution of [24, 22, 27] includes a geometrically-imposed corner-rounding radius. Corner-rounding for a free-boundary problem can be naturally achieved by specifying a curvature dependent surface energy that penalizes the formation of corners and results in corner-rounding [7, 10, 13]. In fact, [26] uses this method to solve the elastic stresses for a void of arbitrary shape and then combines the elasticity solution to find the overall energy-minimizing void shape, as well as dynamics for void shape changes due to mass transport. While such corner-rounding methods permit solution of the elasticity problem because the boundary of the solid is rendered smooth, the corner-rounding also removes the weak (integrable) singularity of the stress at the corner [29]. Of particular interest to us is how the stress singularity of the corner does or does not modify the behavior of the free boundary problem.[5, 30]

The role of a singularity in the elastic stress energy density near a corner could in principle contribute to the energy balance determining the free boundary equilibrium shape and potentially modify the equilibrium corner angle. In the absence of elastic stress, the corner angle on an equilibrium shape is given by a specific condition [3, 4]. [28] consider the elastic energy locally near the corner and use scaling arguments to argue that stresses do not modify the corner angle from the no-stress results. In contrast, [26] consider the energy-minimization problem for the shape of a void in an elastic solid with anisotropic surface energy by using a corner energy regularization term in which there is an energy penalty for corners, and find that the apparent corner angle does depend on elastic stress. So, to resolve the apparent discrepancy in the influence of elastic stress on corners of energy-minimizing free-boundary void shapes, we develop here a reliable numerical method with high accuracy to determine the stress distribution of a void with corners. These results are useful on their own, as a contribution to understanding stress distribution due to voids with specific geometries, and also as a necessary component in the more general problem of finding the energy-

minimizing void shape and understanding the fundamental problem of the effect of elasticity on equilibrium corner angles.

The organization of the paper is as follows: in Section 2, we derive a boundary integro-differential equation from the mathematical formulation of the elasticity problem in an infinite plate under biaxial stress; in Section 3 we describe the numerical method to discretize the integro-differential equation in Section 2; in Section 4, we give examples of the numerical results corresponding to hole shapes with and without corners and analyze the error. Section 5 includes a discussion of our numerical method and conclusion.

2 Mathematical formulation

2.1 Boundary integro-differential equation

We follow Muskhelishvili's complex variable formulation for two-dimensional elasticity [19, 21]. We consider the exterior elasticity problem with a simply connected void and biaxial stress applied at infinity. We assume plane-strain elasticity in the xy -plane. The displacement field in the elastic solid is $\mathbf{u}(x, y) = u_1(x, y)\mathbf{e}_1 + u_2(x, y)\mathbf{e}_2$, where \mathbf{e}_1 and \mathbf{e}_2 are unit vectors in the x, y directions. Let D denote the solid region, D' denote the void region, and let ∂D represent the interface between void and solid. Displacements and the stress tensor are defined on D and ∂D .

The infinitesimal strain tensor is defined by $E = \frac{1}{2}(\nabla \mathbf{u} + \nabla \mathbf{u}^T)$, and the first Piola-Kirchhoff stress tensor for the linearly elastic solid is given by $P = \lambda(\text{tr}(E))I + \mu(E + E^T)$, where $\text{tr}(E)$ is trace of matrix E , I is the identity tensor, and where λ and μ are the Lamé coefficients. Thus,

$$P = \begin{pmatrix} \sigma_x & \tau_{xy} \\ \tau_{xy} & \sigma_y \end{pmatrix} \quad (1)$$

in the xy -plane with far-field condition:

$$\begin{pmatrix} \sigma_x & \tau_{xy} \\ \tau_{xy} & \sigma_y \end{pmatrix} \rightarrow \begin{pmatrix} 1 & 0 \\ 0 & \chi \end{pmatrix} \quad \text{as } \sqrt{x^2 + y^2} \rightarrow \infty, \quad (2)$$

where $\chi = \sigma_1/\sigma_2$ is a parameter after nondimensionalizing the stress components by the x -component of the applied biaxial stress. Mechanical equilibrium in the solid gives (here x_1, x_2 are x, y):

$$\nabla \cdot P = \sum_{i,j=1,2} \frac{\partial P_{ij}}{\partial x_j} \mathbf{e}_i = 0, \quad (3)$$

$$P \cdot \mathbf{n} = 0 \quad \text{on } \partial D, \quad (4)$$

where \mathbf{n} is the unit normal vector exterior to solid. Introduce the stress function $W(x, y)$ as a smooth function defined on D and ∂D , such that $\sigma_x = \partial^2 W / \partial y^2$, $\tau_{xy} = -\partial^2 W / \partial x \partial y$, $\sigma_y = \partial^2 W / \partial x^2$ (see [12]). Then Eq. (3) is satisfied. The compatibility condition for strain dictates that $W(x, y)$ satisfies the biharmonic equation:

$$\frac{\partial^4 W}{\partial x^4} + 2 \frac{\partial^4 W}{\partial x^2 \partial y^2} + \frac{\partial^4 W}{\partial y^4} = 0. \quad (5)$$

Then using two functions $\phi(z)$ and $\psi(z)$ (called Goursat functions) which are holomorphic on D and ∂D to represent $W(x, y)$ with complex variable $z = x + iy$, we let $W(x, y) =$

$\text{Re}\{\bar{z}\phi(z) + \varsigma(z)\}$, and $\psi(z) = \varsigma'(z)$. The relations between the stress components and Goursat functions are then

$$\sigma_x + \sigma_y = 4\text{Re}\{\phi'(z)\}, \quad (6)$$

$$\sigma_y - \sigma_x + 2i\tau_{xy} = 2[\bar{z}\phi''(z) + \psi'(z)]. \quad (7)$$

Substituting Eq. (6), (7) into Eq. (2), the boundary conditions at infinity in terms of ϕ and ψ become

$$\phi(z) = \frac{1+\chi}{4}z + C_1zi + C_2 + O\left(\frac{1}{z}\right) \quad \text{as } |z| \rightarrow \infty, \quad (8)$$

$$\psi(z) = \frac{\chi-1}{2}z + C_3 + O\left(\frac{1}{z}\right) \quad \text{as } |z| \rightarrow \infty, \quad (9)$$

where C_1 is arbitrary real constant and C_2, C_3 are arbitrary complex constants. To make the solution unique and for convenience, we choose these arbitrary constants in ϕ and ψ to be zero, which does not affect the stresses (see [21, 26]). Since no external force is applied on ∂D , the boundary condition on ∂D is given by

$$\phi(z) + z\overline{\phi'(z)} + \overline{\psi(z)} = 0 \quad \text{on } z \in \partial D. \quad (10)$$

The Goursat functions ϕ, ψ can be written as $\phi(z) = (1+\chi)z/4 + \varphi(z)$ and $\psi(z) = (\chi-1)z/2 + h(z)$. Substitute into Eq. (10) and take the conjugate on both sides, then far-field conditions Eq. (8), (9) and boundary condition Eq. (10) are equivalent to

$$\varphi(z) \rightarrow 0 \quad \text{as } |z| \rightarrow \infty, \quad (11)$$

$$h(z) \rightarrow 0 \quad \text{as } |z| \rightarrow \infty, \quad (12)$$

$$\overline{\varphi(z)} + \frac{1+\chi}{4}\bar{z} + \overline{\varphi'(z)} + \frac{1+\chi}{4} + h(z) + \frac{\chi-1}{2}z = 0 \quad \text{on } z \in \partial D. \quad (13)$$

The purpose of making the substitution is to remove the singularity of ϕ and ψ at ∞ . Then φ and h are analytic on the region $D \cup \infty$. Multiply both sides of Eq. (13) by the factor $1/2\pi i \cdot dz/(z-t)$, where t is an arbitrary point in D' , and integrate along boundary ∂D , denoting the integration contour L as ∂D traversed in the counterclockwise direction. Since φ and h are analytic on the region $D \cup \infty$ with the conditions at ∞ (Eq. (11), (12)), and z is analytic in D' , by the Cauchy integral formula, the value of the resulting Cauchy integrals are given by

$$\frac{1}{2\pi i} \int_L \frac{\varphi(z)}{z-t} dz = 0, \quad \frac{1}{2\pi i} \int_L \frac{h(z)}{z-t} dz = 0, \quad \frac{1}{2\pi i} \int_L \frac{z}{z-t} dz = t.$$

Eq. (13) then becomes an integral equation which does not involve $h(z)$:

$$\frac{1}{2\pi i} \int_L \frac{\overline{\varphi(z)}}{z-t} dz + \frac{1+\chi}{2\pi i \cdot 2} \int_L \frac{\bar{z}}{z-t} dz + \frac{1}{2\pi i} \int_L \frac{\overline{\varphi'(z)}}{z-t} dz + \frac{\chi-1}{2}t = 0. \quad (14)$$

Now letting $t \rightarrow z_0$, where z_0 is a point on boundary ∂D , the limits of the Cauchy integrals have the following properties:

$$\lim_{t \rightarrow z_0} \frac{1}{2\pi i} \int_L \frac{\overline{\varphi(z)}}{z-t} dz = \frac{1}{2} \overline{\varphi(z_0)} + \frac{1}{2\pi i} \int_L \frac{\overline{\varphi(z)}}{z-z_0} dz, \quad (15)$$

$$\lim_{t \rightarrow z_0} \frac{1}{2\pi i} \int_L \frac{\bar{z}}{z-t} dz = \frac{1}{2} \bar{z}_0 + \frac{1}{2\pi i} \int_L \frac{\bar{z}}{z-z_0} dz, \quad (16)$$

$$\lim_{t \rightarrow z_0} \frac{1}{2\pi i} \int_L \frac{\bar{z}\varphi'(z)}{z-t} dz = \frac{1}{2} \bar{z}_0 \varphi'(z_0) + \frac{1}{2\pi i} \int_L \frac{\bar{z}\varphi'(z)}{z-z_0} dz. \quad (17)$$

All integrals on the right side of Eq. (15)-(17) are in the sense of Cauchy principle value. Thus we obtain a singular boundary integro-differential equation on ∂D :

$$\begin{aligned} \frac{1}{2} \overline{\varphi(z_0)} + \frac{1}{2\pi i} \int_L \frac{\overline{\varphi(z)}}{z-z_0} dz + \frac{1+\chi}{4} \bar{z}_0 + \frac{1+\chi}{4\pi i} \int_L \frac{\bar{z}}{z-z_0} dz \\ + \frac{1}{2} \bar{z}_0 \varphi'(z_0) + \frac{1}{2\pi i} \int_L \frac{\bar{z}\varphi'(z)}{z-z_0} dz + \frac{\chi-1}{2} z_0 = 0. \end{aligned} \quad (18)$$

Once the integro-differential equation is solved for $\varphi(z)$ on the boundary ∂D , Eq. (13) determines h on the boundary. The stress at any point ζ inside solid can then be determined by analytic continuation of boundary values $\varphi(z)$ and $h(z)$ into the domain D using

$$\varphi(\zeta) = \frac{1}{2\pi i} \int_{-L} \frac{\varphi(z)}{z-\zeta} dz, \quad h(\zeta) = \frac{1}{2\pi i} \int_{-L} \frac{h(z)}{z-\zeta} dz. \quad (19)$$

The analytic continuation of φ and h into the domain can then be used to construct the stress tensor P in the solid from Eq. (6), (7).

2.2 Local asymptotic analysis near corners

Goursat function $\varphi(z)$ is smooth along the boundary if the boundary shape of the hole is smooth (with no corners). For a convex void shape with a corner, $\varphi'(z)$ has a singularity at the corner and the stress goes to infinity when z approaches the corner [24, 29]. We analyze the stress asymptotically to determine the order of the singularity as a function of corner angle. By setting the vertex of the corner as the origin, the shape of the boundary of the hole near the corner is a wedge with same angle as the corner angle (see Fig. 1). The biharmonic equation in polar coordinates is given in [27] as

$$\left(\frac{\partial^2}{\partial r^2} + \frac{1}{r} \frac{\partial}{\partial r} + \frac{1}{r^2} \frac{\partial^2}{\partial \theta^2} \right)^2 W = 0, \quad (20)$$

and the corresponding stress components in polar coordinates are given by

$$\sigma_{rr} = \frac{1}{r} \frac{\partial W}{\partial r} + \frac{1}{r^2} \frac{\partial^2 W}{\partial \theta^2}, \quad (21)$$

$$\sigma_{\theta\theta} = \frac{\partial^2 W}{\partial r^2}, \quad (22)$$

$$\sigma_{r\theta} = -\frac{\partial}{\partial r} \left(\frac{1}{r} \frac{\partial W}{\partial \theta} \right), \quad (23)$$

where σ_{rr} is the stress in the radial direction, $\sigma_{\theta\theta}$ is the stress in the θ direction, and $\sigma_{r\theta}$ is the shear stress.

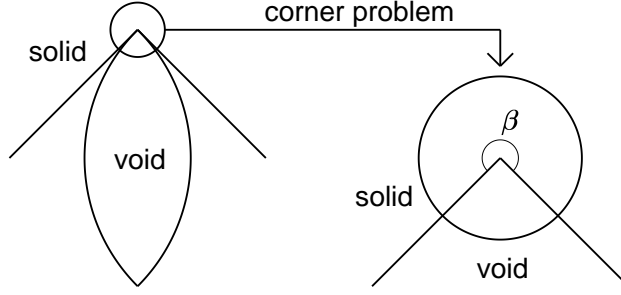


Fig. 1 Boundary shape of the corner problem.

Letting $r = \varepsilon \tilde{r}$ and $W(r, \theta) = \tilde{W}(\tilde{r}, \theta)$ with $\varepsilon \ll 1$ to find the corner solution, the biharmonic Eq. (20) becomes:

$$\frac{1}{\varepsilon^2} \left(\frac{\partial^2}{\partial \tilde{r}^2} + \frac{1}{\tilde{r}} \frac{\partial}{\partial \tilde{r}} + \frac{1}{\tilde{r}^2} \frac{\partial^2}{\partial \theta^2} \right)^2 \tilde{W} = 0. \quad (24)$$

Stresses of the corner problem are:

$$\widetilde{\sigma_{\tilde{r}\tilde{r}}} = \frac{1}{\tilde{r}} \frac{\partial \tilde{W}}{\partial \tilde{r}} + \frac{1}{\tilde{r}^2} \frac{\partial^2 \tilde{W}}{\partial \theta^2} = \varepsilon^2 \sigma_{rr}, \quad (25)$$

$$\widetilde{\sigma_{\theta\theta}} = \frac{\partial^2 \tilde{W}}{\partial \tilde{r}^2} = \varepsilon^2 \sigma_{\theta\theta}, \quad (26)$$

$$\widetilde{\sigma_{r\theta}} = -\frac{\partial}{\partial \tilde{r}} \left(\frac{1}{\tilde{r}} \frac{\partial \tilde{W}}{\partial \theta} \right) = \varepsilon^2 \sigma_{r\theta}, \quad (27)$$

The differential equation of the corner problem is still a biharmonic equation from Eq. (24). Since the far-field conditions $\sigma_{rr}, \sigma_{r\theta}, \sigma_{\theta\theta}$ are finite away from the corner, $\widetilde{\sigma_{rr}}, \widetilde{\sigma_{r\theta}}, \widetilde{\sigma_{\theta\theta}} \rightarrow 0$ as $\tilde{r} \rightarrow \infty$. Hence the local corner problem is identical to the wedge problem. The solution to the wedge problem with “free-free” boundary conditions is given by separation of variables in [29]. The order of φ, φ' and stresses near the corner are

$$\sigma_{rr}, \sigma_{r\theta}, \sigma_{\theta\theta} \sim r^{\lambda-2}, \varphi'(r, \theta) \sim r^{\lambda-2}, \varphi(r, \theta) \sim r^{\lambda-1}, \quad (28)$$

where λ is the solution of

$$\sin [(\lambda - 1)\beta] = -(\lambda - 1) \sin \beta \quad (29)$$

and where β is the corner angle (see Fig. 1). From Eq. (29), we can determine the behavior of the stresses near the corner. In case of $\beta < \pi$, λ is greater than 2 and there is no singularity near the corner. In case of $\beta = \pi$, the boundary is a straight line and the stresses are constant as $\lambda = 2$. When $\pi < \beta < 2\pi$ (see Fig. 1), λ is between 1 and 2 which gives stress singularity near the corner. If β goes to 2π , λ approaches 1. For all cases in which $\pi < \beta < 2\pi$, the singularity in the stresses near the corner is an integrable singularity [29].

3 Numerical method

The surface of the elastic solid is described by a closed continuous curve on the xy -plane. To illustrate and test our numerical method we let the center of the void be the origin and consider two-fold-symmetric void shapes with reflection symmetry across the x and y axes. We consider a class of shapes that are piecewise-smooth except for possible corners on the x and y axes (see Fig. 8 for an illustration). Such corners could be present in the full energy minimization problem for the free boundary shape when the surface energy model is strongly anisotropic with excluded orientations at the corner corresponding to negative surface stiffness [14]. The assumed symmetry of the void shape results in symmetry of the Goursat functions in the complex plane. Thus we consider the shape and the Goursat functions on the first quadrant and use symmetry to extend to the entire xy -plane.

3.1 Modeling the surface

The surface is represented in polar coordinates $r(\theta)$, where r is the radial coordinate and $\theta \in [0, \pi/2]$ denotes the polar angle (note that the polar coordinate is different from Section 2.2). For example, $r(\theta) = 1$ when surface is a circle or $r(\theta) = b/\sqrt{1 - (e \cos \theta)^2}$ for an ellipse with eccentricity e and semi-minor axis b . If the surface is given analytically, $r'(\theta)$ and $r''(\theta)$ can be obtained directly without error. If the surface is not given explicitly, we use a series in Chebyshev polynomials to represent the shape as

$$r(\theta) = \sum_{k=0}^{N-1} c_k T_k(\theta), \quad (30)$$

where $T_k(\theta)$ is the k -th Chebyshev polynomial on $[0, \pi/2]$. Coefficients c_k are derived from the value of r at Chebyshev nodes on $\theta \in [0, \pi/2]$ using Chebyshev interpolation [23]. For cases in which the surface shape is smooth the error can be reduced to machine roundoff error for sufficiently large N . More details about error analysis of Chebyshev interpolation are given in [1].

The problem for the elastic stress distribution has been reduced to an integro-differential equation given by Eq. (18) for the boundary values of the complex function $\varphi(z)$ where $z(\theta) = r(\theta) \cos \theta + i \cdot r(\theta) \sin \theta$. Goursat function φ is holomorphic on D , which leads to φ being a continuous function of θ on the boundary. We use a Chebyshev basis to represent the real and imaginary parts of the boundary values of the Goursat function on the first quadrant:

$$\varphi(\theta) = \sum_{k=0}^{N-1} a_k T_k(\theta) + i \cdot \sum_{k=0}^{N-1} b_k T_k(\theta), \quad (31)$$

where a_k, b_k are unknowns. If the shape of the hole has corners, from the local asymptotic analysis near corners in Section 2.2, the Goursat function φ near the corner can not be well approximated only by polynomials. Thus, considering the example where the corner is located at $\theta_c = \pi/2$, we add a corner term in $s^{\lambda-1}$, where s is the arclength from the corner and λ is the solution of Eq. (29). We thus have $\varphi(\theta) \sim c_1 s^{\lambda-1} \sim c_2 |\theta_c - \theta|^{\lambda-1}$ near the corner where c_1, c_2 are constants. To

accommodate the local behavior near the corner we modify the expansion in Eq. (31) as

$$\varphi(\theta) = a_{N-1} \left(\frac{\pi}{2} - \theta \right)^{\lambda-1} + \sum_{k=0}^{N-2} a_k T_k(\theta) + i \cdot \left(b_{N-1} \left(\frac{\pi}{2} - \theta \right)^{\lambda-1} + \sum_{k=0}^{N-2} b_k T_k(\theta) \right). \quad (32)$$

Using the symmetry of the void shape the associated symmetries of the elastic stress are

$$\begin{aligned} \sigma_x(x, y) &= \sigma_x(-x, y) = \sigma_x(x, -y) = \sigma_x(-x, -y), \\ \sigma_y(x, y) &= \sigma_y(-x, y) = \sigma_y(x, -y) = \sigma_y(-x, -y), \\ \tau_{xy}(x, y) &= -\tau_{xy}(-x, y) = \tau_{xy}(-x, -y) = -\tau_{xy}(x, -y). \end{aligned}$$

Thus, from the dependence of the stress on the Goursat functions we have that $\text{Re}\{\varphi(\theta)\}$ is odd in x and even in y while $\text{Im}\{\varphi(\theta)\}$ is even in x and odd in y . We can use the symmetry to extend $\varphi(\theta)$ on $0 < \theta < \pi/2$ to $\pi/2 < \theta < 2\pi$ as

$$\begin{aligned} \varphi(\theta) &= -\text{Re}\{\varphi(\pi - \theta)\} + i \cdot \text{Im}\{\varphi(\pi - \theta)\} \quad \text{on } \theta \in [\pi/2, \pi]. \\ \varphi(\theta) &= -\text{Re}\{\varphi(\theta - \pi)\} - i \cdot \text{Im}\{\varphi(\theta - \pi)\} \quad \text{on } \theta \in [\pi, 3\pi/2]. \\ \varphi(\theta) &= \text{Re}\{\varphi(2\pi - \theta)\} - i \cdot \text{Im}\{\varphi(2\pi - \theta)\} \quad \text{on } \theta \in [3\pi/2, 2\pi]. \end{aligned}$$

Since φ is a continuous function of θ , we have the continuity conditions on both ends of the interval

$$\text{Re}\{\varphi(\theta)\} = 0 \quad \text{at } \theta = \pi/2, \quad (33)$$

$$\text{Im}\{\varphi(\theta)\} = 0 \quad \text{at } \theta = 0. \quad (34)$$

Note that the integro-differential equation (18) admits a homogeneous solution $\varphi_H(z) = iaz + b$, where a is a real constant and b is a complex constant, which corresponds to arbitrary degrees of freedom in the representation of the stress-free state by Goursat functions [19]. However, because of the assumed symmetry of the shape and our resulting symmetry relations for the real and imaginary parts of $\varphi(z)$, the symmetry excludes the homogeneous solution $\varphi_H(z)$ because b has only even symmetry in both x and y , while iaz has only odd symmetry for x and y .

Some more constraints will be discussed in Section 3.4 to ensure that $\varphi(\theta)$ is boundary value of an analytic function.

3.2 Nested Gauss-Legendre quadrature

Traditional Gauss-Legendre quadrature [11] gives an approximation to the integral of function $f(x)$ on the interval $[-1, 1]$ as

$$\int_{-1}^1 f(x) dx = \sum_{i=1}^N \omega_i f(x_i), \quad (35)$$

where x_i are Gauss-Legendre quadrature points and ω_i are corresponding Gauss-Legendre quadrature weights. Gauss-Legendre quadrature is exact for polynomials under degree $2N$ and it converges as $N \rightarrow \infty$ for smooth functions $f(x)$ which can be approximated by polynomials. However, in the corner case, Eq. (32) has the corner term with a non-integer exponent $\lambda - 1$ when the corner angle of the hole $\beta \neq \pi$.

We introduce nested Gauss-Legendre quadrature [2, 15] to improve the convergence of Gauss-Legendre quadrature for the corner term.

As an illustration of the application of nested Gauss-Legendre quadrature we evaluate $\int_0^1 f(x)dx$ with possible integrable singularity near $x = 1$. The nested Gauss-Legendre quadrature algorithm is [2, 15]:

Step 1: Find Gauss-Legendre quadrature points x_i and Gauss-Legendre quadrature weights ω_i on $[0, 1]$ with N quadrature points. Set $a_1 = 0$ and number of iterations $n = 1$.

Step 2: Evaluate $\int_{a_n}^1 f(x)dx$ using Gauss-Legendre quadrature on $[a_n, 1]$.

Step 3: Let $a_{n+1} = (1 + a_n)/2$. Divide $[a_n, 1]$ into two sub-intervals $[a_n, a_{n+1}]$ and $[a_{n+1}, 1]$.

Step 4: Evaluate $\int_{a_n}^{a_{n+1}} f(x) dx$ and $\int_{a_{n+1}}^1 f(x) dx$ using Gauss-Legendre quadrature.

Step 5: Repeat *Step 2-4* until

$$\left| \int_{a_n}^1 f(x) dx - \left[\int_{a_n}^{a_{n+1}} f(x) dx + \int_{a_{n+1}}^1 f(x) dx \right] \right| < \varepsilon,$$

where ε is a prescribed tolerance. Then

$$\int_0^1 f(x) dx = \sum_{i=1}^n \int_{a_i}^{a_{i+1}} f(x) dx + \int_{a_{n+1}}^1 f(x) dx.$$

As a specific test case, we evaluate $\int_0^1 (1-x)^p dx = 1/(p+1)$ with $-1 < p \leq 5$ using both traditional and nested Gauss-Legendre quadrature. Fig. 2 shows the semi-log plot of the error versus p . Traditional Gauss-Legendre quadrature uses a polynomial basis on the given interval to evaluate the integral. Then the quadrature is exact for functions on the polynomial space. When $0 < p < 3$ and p is not integer, traditional Gauss-Legendre quadrature has significant error. Nested Gauss-Legendre quadrature uses a piecewise polynomial to approximate the function near end of the interval and has better performance in this case. In the singular case ($-1 < p < 0$), both methods have significant error but the nested Gaussian quadrature gives substantially smaller errors. Since Eq. (32) has corner terms with non-integer power, we use nested Gauss-Legendre quadrature to evaluate the integrals.

3.3 Discretization of integral equations

Eq. (18) holds for any z_0 on L . We pick $z_0 = z_i = z(\theta_i)$ $i = 1, 2, \dots, N-1$ as collocation points, where $\theta_i = \pi(x_i + 1)/4$ and x_i is the i -th root of degree $(N-1)$ Legendre polynomial P_{N-1} (Gauss-Legendre quadrature points). The choice of the number of collocation points determines the number of unknowns. We implement both real part and imaginary part of Eq. (18) at each z_i ($2(N-1)$ equations) together with two boundary conditions (33) and (34) to give a system of $2N$ equations for a total of $2N$ unknowns a_k, b_k . The integrals in Eq. (18) are evaluated numerically using nested Gauss-Legendre quadrature described in Section 3.2. $\varphi(\theta_i)$ can be obtained from the Chebyshev coefficients by using Clenshaw's recurrence formula from [6] to minimize the truncation error when evaluating the Chebyshev series at the collocation points $\theta = \theta_i$.

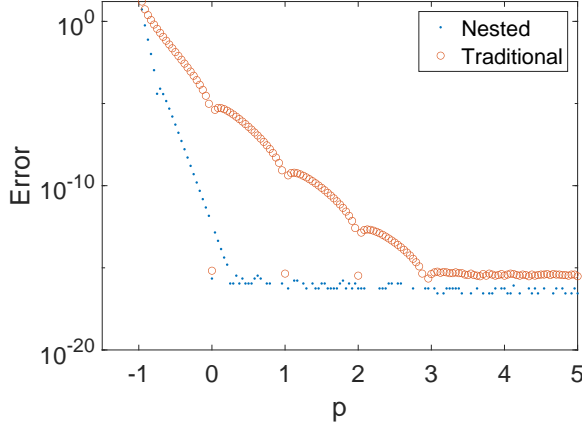


Fig. 2 Comparison of traditional Gauss-Legendre quadrature ($N = 16$) and nested Gauss-Legendre quadrature ($N = 16$ and $\varepsilon = 10^{-15}$) for the integral of x^p on $(0, 1)$.

Now we consider the integrals in Eq. (18) term by term. The singularity of the Cauchy principal value integrals in Eq. (18) is extracted using:

$$\int_L \frac{\overline{\varphi(z)}}{z - z_i} dz = \int_L \frac{\overline{\varphi(z_i)}}{z - z_i} dz + \int_L \frac{\overline{\varphi(z)} - \overline{\varphi(z_i)}}{z - z_i} dz. \quad (36)$$

The first term is

$$\int_L \frac{\overline{\varphi(z_i)}}{z - z_i} dz = \overline{\varphi(z_i)} \cdot \int_L \frac{1}{z - z_i} dz = \pi i \overline{\varphi(z_i)} \quad (37)$$

from boundary version of Cauchy integral formula. The second term takes the form:

$$\int_L \frac{\overline{\varphi(z)} - \overline{\varphi(z_i)}}{z - z_i} dz = \int_0^{2\pi} \frac{\overline{\varphi(\theta)} - \overline{\varphi(\theta_i)}}{z(\theta) - z(\theta_i)} \cdot z'(\theta) d\theta, \quad (38)$$

where

$$z'(\theta) = r'(\theta) \cos \theta - r(\theta) \sin \theta + i(r'(\theta) \sin \theta + r(\theta) \cos \theta).$$

Notice the singularity at $\theta = \theta_i$ is a removable singularity canceled by taking limit at θ_i

$$\lim_{\theta \rightarrow \theta_i} \frac{\overline{\varphi(\theta)} - \overline{\varphi(\theta_i)}}{z(\theta) - z(\theta_i)} = \frac{\overline{\varphi'(\theta_i)}}{z'(\theta_i)}. \quad (39)$$

We find $\varphi'(\theta_i)$ by using the algorithm in [23] based on the relation between the Chebyshev coefficients of a function and the Chebyshev coefficients of its derivatives as

$$c'_{i-1} = c'_{i+1} + 2(i-1)c_i \quad i \geq 1, \quad (40)$$

where c_i are the Chebyshev coefficients and c'_i are Chebyshev coefficient of the derivatives. The Chebyshev coefficients of φ' are linear in unknowns a_k, b_k from Eq. (40). Then integral (36) can be evaluated using nested Gauss-Legendre quadrature and implementing

symmetry of $\varphi(\theta)$ and $r(\theta)$. Continuing with the next integral term in Eq. (18) we evaluate the \bar{z} integral in Eq. (40) the same way, giving

$$\int_L \frac{\bar{z}}{z - z_i} dz = \pi i \bar{z}_i + \int_0^{2\pi} \frac{\bar{z} - \bar{z}_i}{z - z_i} z'(\theta) d\theta. \quad (41)$$

Next we consider the $\bar{z}\varphi'(z)$ term in Eq. (18):

$$\int_L \frac{\bar{z}\varphi'(z)}{z - z_i} dz = \int_L \frac{\bar{z}_i\varphi'(z_i)}{z - z_i} dz + \int_L \frac{\bar{z}\varphi'(z) - \bar{z}_i\varphi'(z_i)}{z - z_i} dz. \quad (42)$$

Following the same logic, the first term is

$$\int_L \frac{\bar{z}_i\varphi'(z_i)}{z - z_i} dz = \pi i \bar{z}_i\varphi'(z_i). \quad (43)$$

Rewriting the second integral in terms of θ gives

$$\int_L \frac{\bar{z}\varphi'(z) - \bar{z}_i\varphi'(z_i)}{z - z_i} dz = \int_0^{2\pi} \frac{\overline{z(\theta)}\varphi'(\theta) - \overline{z(\theta_i)}\varphi'(\theta_i)}{z(\theta) - z(\theta_i)} d\theta. \quad (44)$$

The singularity at $\theta = \theta_i$ is a removable singularity with

$$\lim_{\theta \rightarrow \theta_i} \frac{\overline{z(\theta)}\varphi'(\theta) - \overline{z(\theta_i)}\varphi'(\theta_i)}{z(\theta) - z(\theta_i)} = \frac{z'(\theta_i)\varphi'(\theta_i) + \overline{z(\theta_i)}\varphi''(\theta_i)}{z'(\theta_i)}. \quad (45)$$

Nested Gauss-Legendre quadrature has significant error when function has a singularity. Therefore, Eq. (44) needs to be evaluated carefully near the corner using integration by parts to avoid the singularity of $\varphi'(\theta)$ at $\theta = \pi/2$:

$$\int_0^{\pi/2} \frac{\overline{z(\theta)}\varphi'(\theta)}{z(\theta) - z(\theta_i)} d\theta = \int_0^{\pi/2 - \theta_\varepsilon} \frac{\overline{z(\theta)}\varphi'(\theta)}{z(\theta) - z(\theta_i)} d\theta + \int_{\pi/2 - \theta_\varepsilon}^{\pi/2} \frac{\overline{z(\theta)}\varphi'(\theta)}{z(\theta) - z(\theta_i)} d\theta, \quad (46)$$

$$\int_{\pi/2 - \theta_\varepsilon}^{\pi/2} \frac{\overline{z(\theta)}\varphi'(\theta)}{z(\theta) - z(\theta_i)} d\theta = \left. \frac{\overline{z(\theta)}\varphi(\theta)}{z(\theta) - z(\theta_i)} \right|_{\pi/2 - \theta_\varepsilon}^{\pi/2} - \int_{\pi/2 - \theta_\varepsilon}^{\pi/2} \varphi(\theta) d\left(\frac{\overline{z(\theta)}}{z(\theta) - z(\theta_i)} \right), \quad (47)$$

where $\theta_\varepsilon = \theta_1/2$, and θ_1 is the polar angle at first collocation point.

We substitute all results in this section to discretize Eq. (18). $\varphi(\theta)$ is a linear combination of unknowns a_k and b_k for any θ from Eq. (32). The coefficients of derivative of a Chebyshev approximated function are linear in the coefficients of original Chebyshev approximated function (Eq. (40)), thus $\varphi'(\theta_i)$ and $\varphi''(\theta_i)$ are linear in a_k and b_k . Gauss-Legendre quadrature is a weighted sum of the function values at quadrature points, which is a linear operator in φ or φ' . Finally, we get a linear system of a_k and b_k from discretizing Eq. (18).

3.4 Analyticity equations

In Section 3.1, we assume φ is a smooth function of θ on first quadrant of boundary ∂D from (31). However, φ in Eq. (18) is an analytic function on $D \cup \partial D$. Not every function with smooth real and imaginary part on the boundary is an analytic function. So more constraints are needed to make φ an analytic function in D . Since $\varphi(\zeta)$ is analytic for ζ in D , by the Cauchy integral formula and our requirement that $\varphi(\infty) = 0$ from Eq. (11),

$$\varphi(\zeta) = \frac{1}{2\pi i} \int_{-L}^{\infty} \frac{\varphi(z)}{z - \zeta} dz. \quad (48)$$

Thus,

$$\varphi(\zeta) = \frac{1}{2\pi i} \int_{-L}^{\infty} \frac{\varphi(z)}{z - \zeta} dz \rightarrow 0 \quad \text{as } |\zeta| \rightarrow \infty. \quad (49)$$

Eq. (49) holds because $\varphi(z)$ is bounded on ∂D . This definition of $\varphi(\zeta)$ guarantees analyticity in D . To make $\varphi(\zeta)$ analytic on $D \cup \partial D$, φ should be continuous to any point on boundary ∂D . Since collocation points z_i are on boundary ∂D , $\varphi(\zeta)$ is continuous as $\zeta \rightarrow z_i$ for all i :

$$\lim_{\zeta \rightarrow z_i} \frac{1}{2\pi i} \int_{-L}^{\infty} \frac{\varphi(z)}{z - \zeta} dz = \varphi(z_i). \quad (50)$$

Take the limit and evaluate the integral using its Cauchy principle value, the limit becomes:

$$\frac{1}{2\pi i} \int_L^{\infty} \frac{\varphi(z)}{z - z_i} dz + \frac{1}{2} \varphi(z_i) = 0 \quad (51)$$

for any collocation point z_i . The integral in Eq. (51) can be evaluated in the same way as we find the Cauchy integral of $\varphi(z)$ in section 3.2. Then Eq. (51) at collocation points are a set of linear equations of a_k and b_k . Since Eq. (51) on all points on ∂D enforces the analyticity of $\varphi(\zeta)$ on $D \cup \partial D$, we therefore use Eq. (51) at each collocation point in addition to our boundary integral equation (18) to construct our analytic $\varphi(z)$.

We know that the solution to the two-dimensional elasticity problem is unique [16]. But if we solve Eq. (18) without constraints Eq. (51), other non-analytic φ cause the solution to be non-unique. Eq. (51) at collocation points restricts the solution to the space of boundary values of analytic functions, which ensures the uniqueness of the solution to discretized problem. Finally, by combining the $2(N - 1)$ equations from Eq. (51) at collocation points, the $2(N - 1)$ equations from discretized integral equation Eq. (18), and two equations Eq. (33), (34) from boundary conditions at each end of the domain, we obtain an overdetermined linear system of $(4N - 2)$ equations for the $2N$ unknowns a_k and b_k . The non-square linear system can be solved in sense of least squares using the MATLAB matrix left division operator (QR method).

4 Numerical results

Now we have a numerical method to determine the Goursat function on the boundary. In this section, we test our numerical method on cases for which the boundary shape corresponds to a circle, an ellipse, and overlapping circles.

4.1 Measurements of the error

In the cases of the circle and the ellipse, the exact solution for the Goursat function on the boundary are given in [21]. We can compare φ from our numerical method with exact solution using the L^2 error norm:

$$\text{Error}_{L^2} = \left[\frac{2}{\pi} \int_0^{\pi/2} |\varphi(\theta) - \varphi_{\text{exact}}(\theta)|^2 d\theta \right]^{1/2}. \quad (52)$$

In the case of overlapping circles, there is an exact solution for the trace of the stress $\sigma_x + \sigma_y$ [18] but not for φ . Comparing $\sigma_x + \sigma_y = 1 + \chi + 4\text{Re}\{\varphi'(z)\}$ with the exact solution is a good numerical test for our method. We thus define the L^2 norm error of $\sigma_x + \sigma_y$ as

$$\text{Error}_{L^2} = \left[\frac{2}{\pi} \int_0^{\pi/2} ((\sigma_x + \sigma_y) - (\sigma_x + \sigma_y)_{\text{exact}})^2 d\theta \right]^{1/2}. \quad (53)$$

4.2 Test for circle

When the interface is a unit circle, the exact solution of the interior problem for the case of uniaxial tension, $\chi = 0$, is $\varphi(z) = 2z$. The solution of the exterior problem is derived by the conformal map $z(\zeta) = 1/\zeta$ which maps the interior domain to the exterior domain. Here $r(\theta) = 1$ and $r'(\theta) = r''(\theta) = 0$. The exact solution of exterior problem for the case of uniaxial tension $\chi = 0$ is given by $\varphi_{\text{exact}}(z) = 1/(2z)$ [21]. Absolute values of the computed Chebyshev coefficients for $\varphi(z)$, a_k and b_k , are presented in Fig. 3. Coefficients of $\varphi(z)$ decrease to magnitudes comparable to the truncation error at $N = 15$ which confirms the convergence of our collocation method. The convergence rate is shown in the L^2 error versus N plot in Fig. 4. These results verify that our numerical algorithm has spectral convergence in the number of collocation points N when the boundary shape is a unit circle.

4.3 Test for ellipse

An ellipse in the complex z -plane can be conformally mapped to the interior circle problem in the ζ -plane with $z(\zeta) = 1/\zeta + m\zeta$ for $0 < m < 1$. Thus, the exact solution for $\chi = 0$ is $\varphi(z) = (1 - m)/\zeta$ [21]. The exact solution for the ellipse when $m = 0.5$ is shown in Fig. 5.

We test our numerical method for the ellipse with the eccentricity

$$e = \sqrt{1 - (1 - m)^2/(1 + m)^2}. \quad (54)$$

The equation of the ellipse in polar coordinates is

$$r(\theta) = (1 - m)/\sqrt{1 - (e \cos \theta)^2}. \quad (55)$$

We can get $r'(\theta)$ and $r''(\theta)$ by taking the derivatives:

$$r'(\theta) = -\frac{1 - m}{2} (1 - e^2 \cos^2 \theta)^{-3/2} e^2 \sin 2\theta, \quad (56)$$

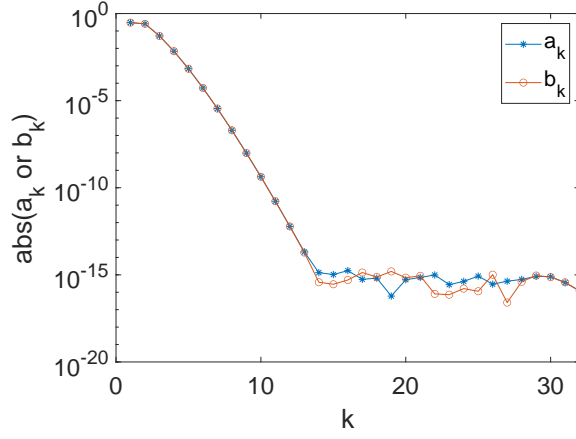


Fig. 3 Result for test case of a circle: absolute value of coefficient of a_k or b_k versus index k for the number of collocation points $N = 32$.

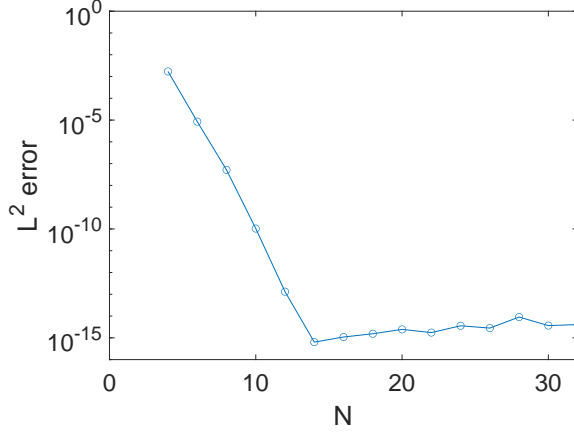


Fig. 4 Result for test case of a circle: L^2 error of $\varphi(z)$ versus number of collocation points N . Here L^2 error is defined in Section 4.1.

$$r'''(\theta) = -\frac{1-m}{2}[-(3/2) \cdot (1 - e^2 \cos^2 \theta)^{-5/2} \cdot (e^2 \sin 2\theta)^2 + 2(1 - e^2 \cos^2 \theta)^{-3/2} e^2 \cos 2\theta]. \quad (57)$$

The calculated Chebyshev coefficients when $m = 0.5$ are given in Fig. 6. Fig. 7 shows that the numerical solution converges rapidly and has error comparable to the truncation error when $N > 50$. Thus, our numerical method converges rapidly for the smooth-boundary test cases of a circle and an ellipse.

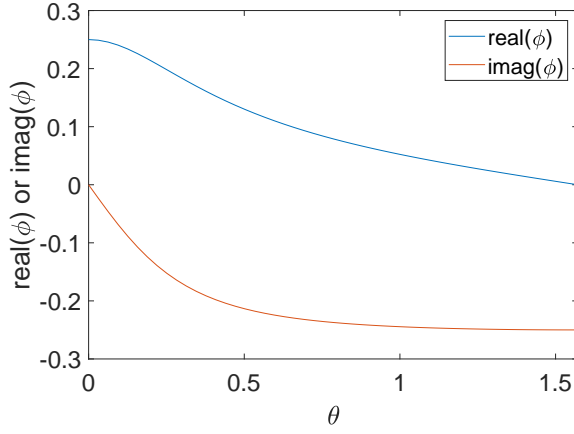


Fig. 5 Real part and imaginary part of exact solution φ_{exact} versus $\theta \in [0, \pi/2]$ when $m = 0.5$.

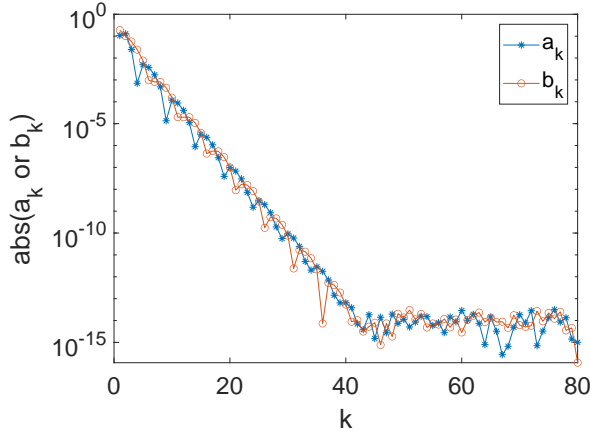


Fig. 6 Result for test case of an ellipse: Absolute value of coefficients of a_k or b_k versus k when number of collocation points $N = 80$.

4.4 Test for overlapping circles ($\alpha = \pi/3$)

In this test, we show the convergence of the numerical method when the shape has corners. Consider the shape formed by two overlapping circles with the same radius (see Fig. 8). The void shape is given by taking the $x > 0$ portion of the unit circle with center at $(\cos(\alpha), 0)$ and reflecting it across the y axis. Thus the parameter α controls the amount of overlap between the circles. There are three cases: (i) the degenerate case corresponding to a single unit circle occurs for $\alpha = \pi/2$; (ii) the "separating circles" case for $0 \leq \alpha < \pi/2$ as illustrated in Fig. 8; and (iii) the "collapsing circles" case for $\pi/2 < \alpha < \pi$ as illustrated in Fig. 12. In this test, we consider the "separating circles" case with $\alpha = \pi/3$ for which the void shape has two inward-pointing corners on the y axis. Since the shape has corners, we apply Eq. (32) to represent $\varphi(\theta)$ in our numerical method. The order of the corner term has $\lambda = 2.0465$ which is the solution to Eq. (29)

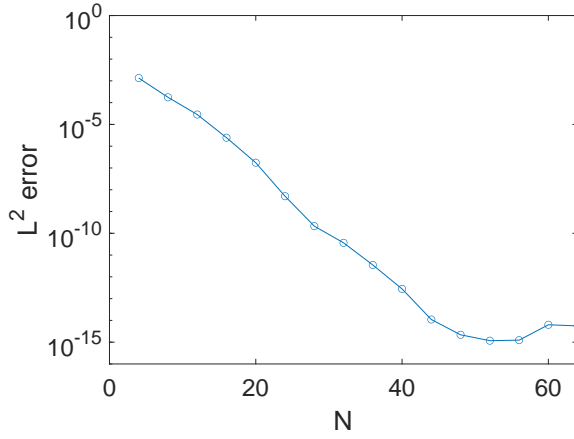


Fig. 7 Result for test case of an ellipse: L^2 error of $\varphi(z)$ versus number of collocation points N . Here L^2 error is defined in Section 4.1.

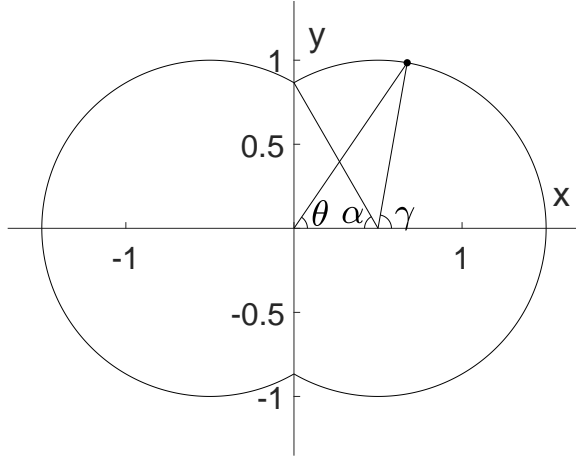


Fig. 8 Overlapping circles shape when $\alpha = \pi/3$.

with corner angle $\beta = 2\alpha$. Consistent with [29], if the corner angle of the solid is less than π , there will be no singularity in the stress at the corner.

The exact solution of $\sigma_x + \sigma_y$ in this overlapping circles shape is given in [18]. The equation of the shape in polar coordinates is $r(\theta) = \cos \alpha \cos \theta + \sqrt{1 - \sin^2 \theta \cos^2 \alpha}$ in the first quadrant. The exact solution for $\sigma_x + \sigma_y$ is given in [18] by an integral

$$\sigma_x + \sigma_y = 4(\cosh \xi - \cos \alpha) \sin \alpha \times \int_0^\infty \frac{2K - (N_1 - N_2)s(s - \cot \alpha \coth s\alpha)}{\sinh 2s\alpha + s \sin 2\alpha} \times \sinh s\alpha \cos s\xi ds, \quad (58)$$

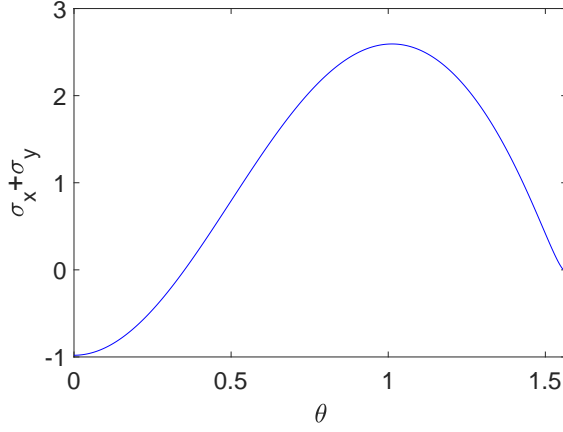


Fig. 9 Exact solution of overlapping circles shape: $\sigma_x + \sigma_y$ versus $\theta \in [0, \pi/2)$ when $\alpha = \pi/3$ and the far-field stress parameter $\chi = 0$.

where K is the solution of the equation

$$4K \int_0^\infty \frac{\sinh^2 s\alpha - s^2 \sin^2 \alpha}{s(s^2 + 1)(\sinh 2s\alpha + s \sin 2\alpha)} ds + 2(N_1 - N_2) \int_0^\infty \frac{s \sin^2 \alpha}{\sinh 2s\alpha + s \sin 2\alpha} du = N_1, \quad (59)$$

where ξ is defined by

$$\cosh \xi = \frac{1 + \cos \alpha \cos \gamma}{\cos \alpha + \cos \gamma}, \quad (60)$$

$\gamma = \theta + \arcsin(\sin \theta \cos \alpha)$ is the center angle (see Fig. 8), N_1 is the tension parallel to the x -axis and N_2 is the tension parallel to the y -axis. The value of $\sigma_x + \sigma_y$ for the exact solution is evaluated using the MATLAB numerical integration function 'integral' [25]. The exact solution for $\sigma_x + \sigma_y$ is shown in Fig. 9 for the overlapping circles case with $\alpha = \pi/3$ and longitudinal tension ($N_1 = 1$ and $N_2 = 0$, corresponding to $\chi = 0$). The accuracy of the numerical integration near the corner has been verified by comparing to the asymptotic behavior of the integral near the corner. Derivation of the asymptotic behavior of the integral is given in Appendix A.

We test our numerical method for the overlapping circles case $\alpha = \pi/3$ for the uniaxial tension case $\chi = 0$. Fig. 10 and Fig. 11 demonstrate that our numerical method works when the shape of the hole has a corner with angle greater than π . Fig. 10 shows that the magnitude of the coefficients a_k and b_k decays to 10^{-10} for $N = 64$ and Fig. 11 shows that the L^2 error of $\sigma_x + \sigma_y$ is about 10^{-5} when N is larger than about 45. While the result is not as accurate as the results for smooth shapes in Section 4.2 and Section 4.3, the accuracy is still very good for relatively small N . See Section 4.7 for a discussion of the error.

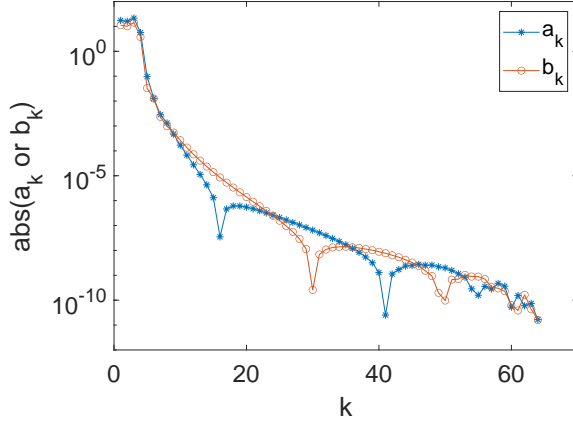


Fig. 10 Overlapping circles with $\alpha = \pi/3$ and $\chi = 0$: Absolute value of coefficients of a_k or b_k versus k when number of collocation points $N = 64$.

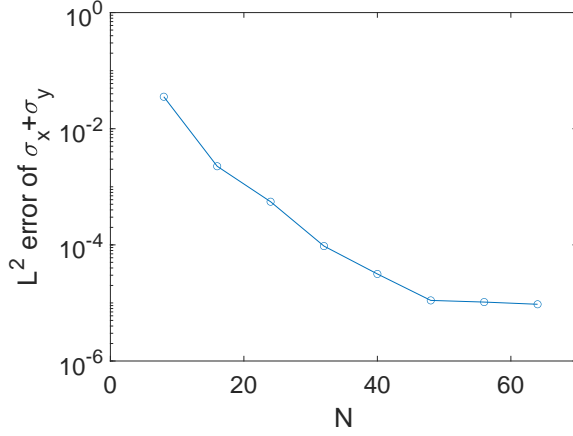


Fig. 11 Overlapping circles with $\alpha = \pi/3$ and $\chi = 0$: L^2 error of $\sigma_x + \sigma_y$ versus number of collocation points N .

4.5 Test for overlapping circles ($\alpha = 2\pi/3$)

We show the effect of the corner term in Eq. (32) in this test. The shape of "collapsing" overlapping circles when $\alpha = 2\pi/3$ is shown in Fig. 12. When the hole shape has corners with corner angle less than π , the stress has a singularity at the corner [29]. If we use the expansion (31) for $\varphi(\theta)$ without the corner term the result is as shown in Figs. 13 and 14. The error of $\sigma_x + \sigma_y$ is large near the corner at $\theta = \pi/2$. Expansion (31) uses a set of polynomials to approximate a $\varphi(\theta)$ that has a discontinuous derivative at the end of the interval. Thus, oscillations are expected near the point of discontinuity (Runge's phenomenon [9]).

We can reduce the error by introducing the corner term in $\varphi(\theta)$ as given in Eq. (32). The order of the corner term $\lambda - 1$ can be obtained by Eq. (29) using the known value

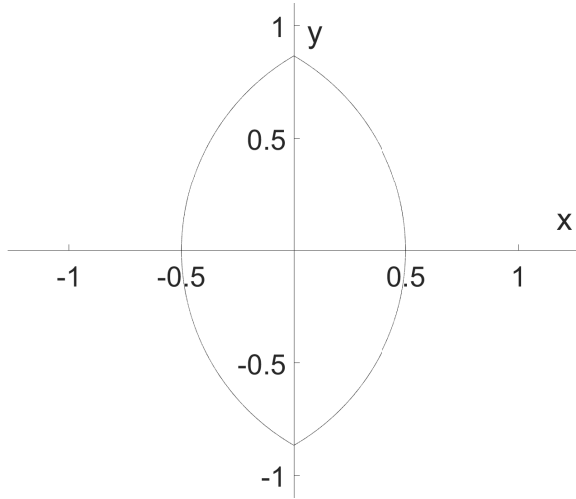


Fig. 12 Overlapping circles shape when $\alpha = 2\pi/3$.

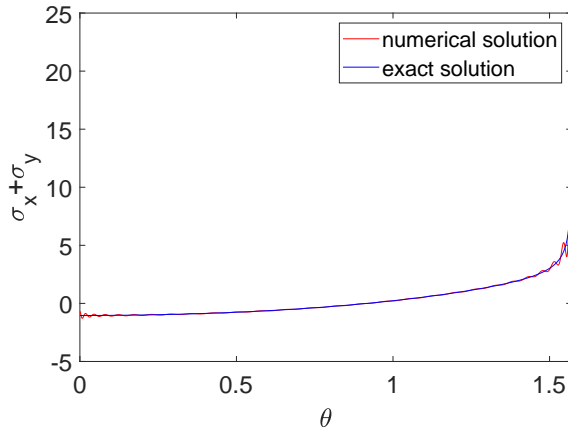


Fig. 13 Overlapping circles case ($\alpha = 2\pi/3$), no corner term: Numerical solution and exact solution of $\sigma_x + \sigma_y$ versus $\theta \in [0, \pi/2)$. Parameters are $N = 64$, $\chi = 0$.

of the corner angle β . Example numerical results for $N = 64$ are shown in Figs. 15-17. Comparing the magnitude of the error to the magnitude of the solution near the corner we note that the maximum of the relative error is less than 10^{-3} approaching the corner. Fig. 18 shows the L^2 error of $\sigma_x + \sigma_y$ versus number of collocation points. The L^2 error is less than 10^{-4} when N is large, which is comparable to the error magnitude for the nonsingular case. So, even in this case with a stress singularity near the corner, the numerical solution is of good accuracy for moderately large N .

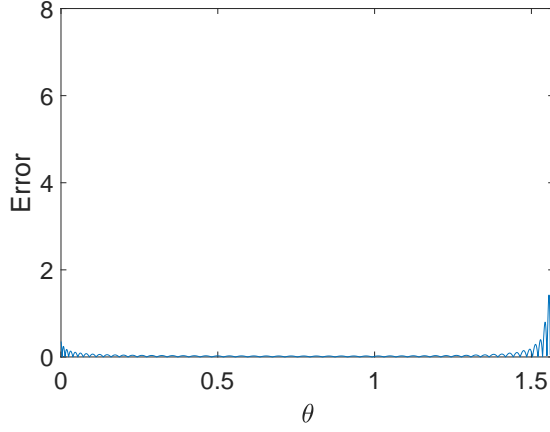


Fig. 14 Overlapping circles case ($\alpha = 2\pi/3$), no corner term: Error of $\sigma_x + \sigma_y$ versus $\theta \in [0, \pi/2)$. Parameters are $N = 64$, $\chi = 0$.

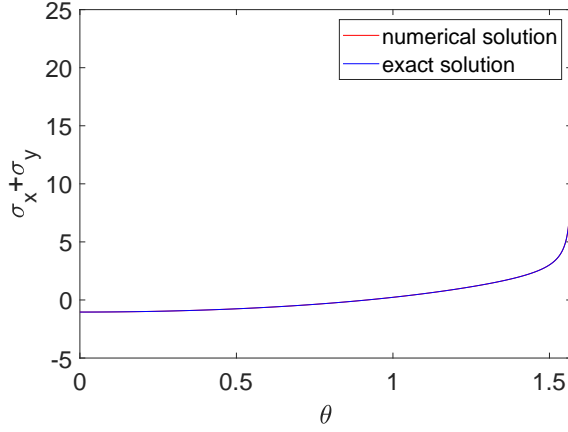


Fig. 15 Overlapping circles case ($\alpha = 2\pi/3$) with corner terms: Numerical solution and exact solution of $\sigma_x + \sigma_y$ versus $\theta \in [0, \pi/2)$. Parameters are $N = 64$, $\chi = 0$.

4.6 Contour plots of stresses

Our numerical method gives the boundary value of φ with small error. We can find the boundary value of the analytic function $h(z)$ on ∂D with small error by Eq. (13). Then analytic functions φ, h can be extended to any ζ in D by Cauchy's integral formula:

$$\varphi(\zeta) = \frac{1}{2\pi i} \int_{-L}^L \frac{\varphi(z)}{z - \zeta} dz, \quad h(\zeta) = \frac{1}{2\pi i} \int_{-L}^L \frac{h(z)}{z - \zeta} dz. \quad (61)$$

The integral is evaluated using by MATLAB numerical integration function since there is no singularity if ζ is not on the boundary. From $\varphi(\zeta)$ and $h(\zeta)$ in D we can determine the stresses at any point in D using Eqs. (6)-(7), where we apply the finite difference

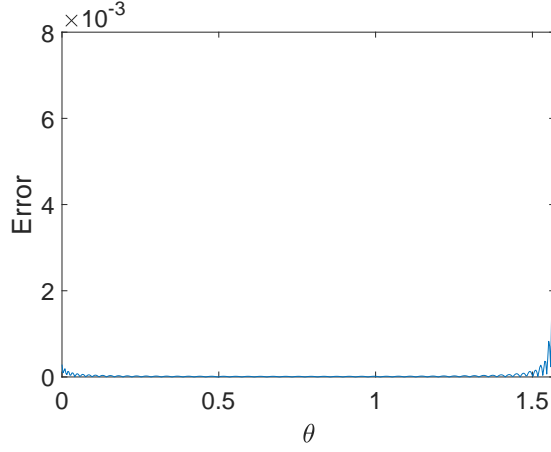


Fig. 16 Overlapping circles case ($\alpha = 2\pi/3$) with corner terms: Error of $\sigma_x + \sigma_y$ versus $\theta \in [0, \pi/2)$. Parameters are $N = 64$, $\chi = 0$.

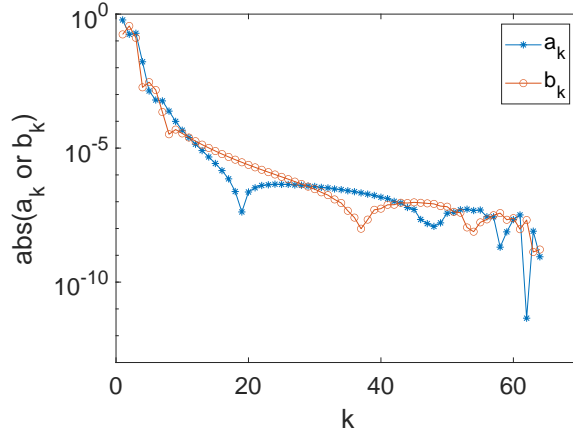


Fig. 17 Overlapping circles case ($\alpha = 2\pi/3$) with corner terms: Absolute value of coefficient of a_k or b_k versus index k . Parameters are $N = 64$, $\chi = 0$.

method with small step size to evaluate the derivatives of φ and h . Fig. 19 illustrates the results for the stress distribution for the overlapping circles case.

4.7 Error analysis

From our numerical results for the cases of the circle and ellipse, we see in these smooth boundary cases our numerical method gives spectral convergence. In this case, both real and imaginary parts of the Goursat function are smooth and thus can be well approximated by Chebyshev series. Nested Gaussian quadrature achieves spectral convergence for the numerical integration, and analyticity constraints Eq. (51)

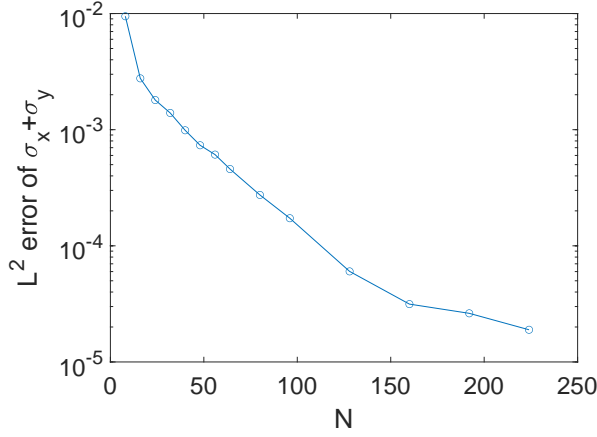


Fig. 18 Overlapping circle case ($\alpha = 2\pi/3$) with corner terms: L^2 error of $\sigma_x + \sigma_y$ versus number of collocation points N for $\chi = 0$.

guarantee that φ must correspond to boundary values of an analytic function which ensure the correctness and uniqueness of the solution.

In the case with the non-smooth shape, the numerical solution is close to the exact solution with L^2 error less than 10^{-4} even when the stresses have singularities near the corner. We argue that this error is a combination of not completely resolving the non-analytic behavior near the corner and poor conditioning of the discretized system. The nonanalytic term in the expansion Eq. (32) was derived from asymptotic analysis near the corner. While we capture the dominant behavior of the singularity with the corner term in Eq. (32), we do not capture other non-integer powers in the expansion of the wedge solution [29], and thus we would not expect to recover the exact solution near the corner. These other non-integer powers could be determined from the higher-order solutions to Eq. (29) (which is the same as Eq. (77) that could be used to find the sub-dominant terms in our asymptotic expansion of the exact solution in Appendix A).

Another contribution to the error is due to poor conditioning. Since the corner term in Eq. (32) is not orthogonal to Chebyshev polynomials, there is some redundancy in the expansion which makes the matrix problem from collocation method somewhat ill-conditioned due to the lack of independence of the corner coefficient a_{N-1} and the coefficients of the regular Chebyshev expansion. It may be possible in a future work to use the wedge solution to give not only the power but also the coefficient of this corner term from the asymptotic analysis. In this case, by determining the a_{N-1} coefficient from the asymptotic analysis, the resulting regular Chebyshev expansion would be used to fit $\varphi - a_{N-1}(\pi/2 - \theta)^{\lambda-1}$ which would be better conditioned. If we have to retain the corner term as a term with an unknown coefficient, then to accurately reproduce the non-integer power series in the vicinity of the corner, and remove the ill-conditioning of the current matrix, we could consider developing an orthogonal basis based on the non-integer power from the corner singularity.

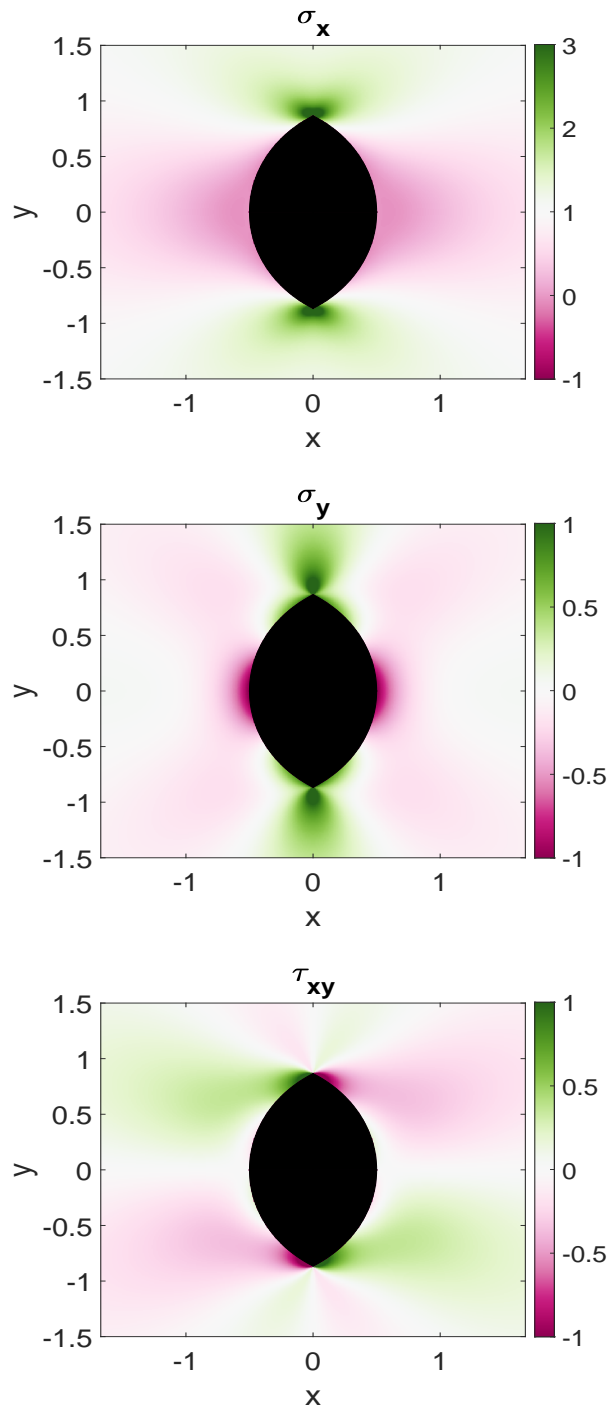


Fig. 19 Distribution of stresses for overlapping circles case with $\alpha = 2\pi/3$, $\chi = 0$. Note the exact stress may exceed the range of the color bar due to the singularity at the corner.

5 Summary

We developed a numerical method to determine the elastic stresses around a hole in an infinite plate. Our numerical method is based on the boundary integro-differential equations obtained using complex Goursat functions. We represent the real and imaginary part of the boundary value of the complex Goursat function φ by a series of Chebyshev polynomials with possible corner terms. The corner term is chosen based on the asymptotic analysis of the stress near the corner and captures the dominant (possibly singular) behavior of the stress. The boundary integro-differential equation is solved numerically using the collocation method at Gauss-Legendre collocation points. To improve the accuracy of the numerical method, we separate the singularity in the integro-differential equation and evaluate the remaining parts by nested Gaussian quadrature. The boundary equation for φ is augmented by analyticity constraints to ensure φ is an analytic function in the solid. Then we solve the over-determined system of the integro-differential equations, end of the interval conditions together with analyticity constraints to determine the boundary value of φ . For the case of a smooth boundary shape, our numerical method converges to the exact solution spectrally with a small number of collocation points. For the case when the boundary shape has a corner, our numerical method includes a corner term derived from asymptotic analysis of the stress singularity at the corner. In this case we obtain elastic stresses accurate to relative error less than 10^{-3} . Finally, we obtain the distribution of stresses in the solid by taking the Cauchy integral of the Goursat function on the boundary of the hole.

In the present work, we make use of the corner angle to determine the asymptotic behavior of the stress singularity in the vicinity of a corner and use this asymptotic behavior to modify our numerical method. While the results presented here demonstrate the approach for only a single corner in our computational domain, the ideas could be extended to handle multiple corners in a straightforward way. Also, we make use of an assumed two-fold symmetry for the shape to reduce the number of unknowns for the integral equation for the Goursat function φ and to eliminate the homogenous solution. For holes with asymmetric shape these symmetry assumptions could be relaxed. In the asymmetric case the shape and the Goursat function could be represented on the interval $0 \leq \theta \leq 2\pi$ using an appropriate spectral representation.

The independence of analyticity constraints in Section 3.4 deserves further attention. Eq. (32) at collocation points adds $2N - 2$ equations to the linear system to ensure the analyticity which causes the linear system to be over-determined. If we formulate the integral equations in a way that the solution for φ is guaranteed to be the boundary value of an analytic function (see, for example [19]), the size of the linear system can be reduced to about half as large as before which would speed up the numerical method considerably.

Appendix A: Asymptotic analysis near the corner for overlapping circles case.

Here we derive the asymptotic behavior of the stress near the corner for the overlapping circle case of Section 4.5. The trace of the stress tensor for the overlapping circles case is given by Eq. (58) which we write as

$$\sigma_x + \sigma_y = H(\xi, \alpha) \int_0^\infty F(s, \alpha) \cos s\xi ds, \quad (62)$$

where

$$H(\xi, \alpha) = 4(\cosh \xi - \cos \alpha) \sin \alpha, \quad (63)$$

$$F(s, \alpha) = \frac{2K - (N_1 - N_2)s(s - \cot \alpha \coth s\alpha)}{\sinh 2s\alpha + s \sin 2\alpha} \cdot \sinh s\alpha \quad (64)$$

with

$$\cosh \xi = \frac{1 + \cos \alpha \cos \gamma}{\cos \alpha + \cos \gamma} \quad (65)$$

and

$$\gamma = \theta + \arcsin(\sin \theta \cos \alpha). \quad (66)$$

Here, the polar angle from the center of the circle γ , polar angle θ , amount of overlap between the circles α , tensions N_1 and N_2 are defined as in Section 4.4. We use $\alpha = 2\pi/3$ as an example in this Appendix. The result can be generalized to other α in $\pi/2 < \alpha < \pi$ using a similar approach as described here. The corner location is at $\theta = \pi/2$. As $\theta \rightarrow \pi/2$, $\gamma \rightarrow \pi/2 + \arcsin(\cos \alpha)$. Thus,

$$\cos \gamma \rightarrow \cos[\pi/2 + \arcsin(\cos \alpha)] = -\cos \alpha. \quad (67)$$

So

$$\cosh \xi = \frac{1 + \cos \alpha \cos \gamma}{\cos \alpha + \cos \gamma} \rightarrow \infty, \quad (68)$$

which gives $\xi \rightarrow \infty$ as $\theta \rightarrow \pi/2$. Thus the $\cos(s\xi)$ term in integral (62) is highly oscillatory near the corner which may cause inaccuracy of the numerical integration.

We determine the behavior of the integral near the corner by applying asymptotic analysis. Let $\theta = \pi/2 - \varepsilon$ where $0 < \varepsilon \ll 1$ then $\cos \theta = \sin \varepsilon = \varepsilon - \varepsilon^3/6 + \mathcal{O}(\varepsilon^5)$ and $\sin \theta = \cos \varepsilon = 1 - \varepsilon^2/2 + \mathcal{O}(\varepsilon^4)$. By Eq. (66), we have

$$\cos \gamma = \cos \theta \sqrt{1 - \sin^2 \theta \cos^2 \alpha} - \sin^2 \theta \cos \alpha. \quad (69)$$

Thus we have

$$\cos \gamma = -\cos \alpha + \varepsilon \sin \alpha + \mathcal{O}(\varepsilon^2). \quad (70)$$

Substitute Eq. (70) into Eq. (68), the asymptotic approximation of $\cosh \xi$ is

$$\cosh \xi = \frac{e^\xi + e^{-\xi}}{2} = \frac{1}{\varepsilon} \sin \alpha + \cos \alpha + \mathcal{O}(\varepsilon). \quad (71)$$

Thus,

$$\xi = \ln \left[\frac{2}{\varepsilon} \sin \alpha + 2 \cos \alpha + \mathcal{O}(\varepsilon) \right], \quad (72)$$

Now consider the integral in (62). F has properties $F(-s) = F(s)$, $F(s) \rightarrow 0$ as $s \rightarrow \pm\infty$ and $F(s, \alpha)$ is bounded for all s ($s = 0$ is a removable singularity), so we can rewrite the integral on $-\infty < s < +\infty$ as

$$I = \int_0^\infty F(s, \alpha) \cos s\xi ds = \frac{1}{2} \int_{-\infty}^\infty F(s, \alpha) \cos s\xi ds. \quad (73)$$

We evaluate I by considering the contour integral on complex plane $z = s + it$:

$$\tilde{I} = \lim_{R \rightarrow \infty} \int_C F(z, \alpha) e^{i\xi z} dz, \quad (74)$$

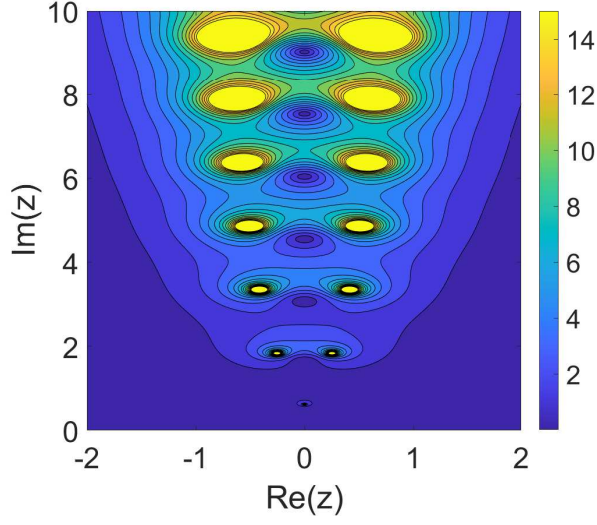


Fig. 20 Contour plot of $|F|$ on upper half plane for $\alpha = 2\pi/3$.

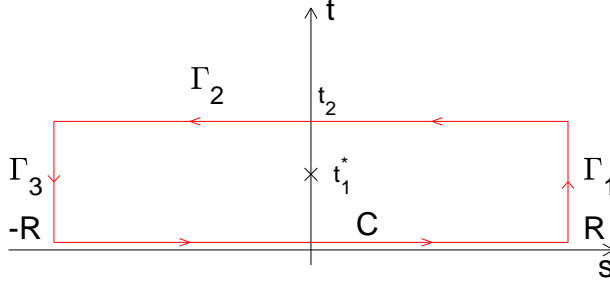


Fig. 21 Complex contour integral.

$$I = \frac{1}{2} \text{Re}\{\tilde{I}\}, \quad (75)$$

where C is the line along s axis from $-R$ to R . $F(z, \alpha)$ is analytic in upper half plane $\text{Im}(z) > 0$ except zeros of the denominator located by the roots of

$$\sinh 2z\alpha + z \sin 2\alpha = 0. \quad (76)$$

There are infinitely many singularities of $F(z, \alpha)$ on the upper half plane (see Fig. 20). We claim that since \tilde{I} contains $e^{i\xi z} = e^{-\xi t} e^{i\xi s}$ and $\xi \gg 1$, the integral \tilde{I} can be approximated by the contribution from the residual of the singularity that occurs at the location with smallest imaginary part t in the upper half plane. For $\alpha = 2\pi/3$, as shown in Fig. 20, this first singularity lies on the imaginary axis, and so satisfies $s = 0$ and

$$\sin 2\alpha t + t \sin 2\alpha = 0. \quad (77)$$

For $\alpha = 2\pi/3$ the solution of Eq.(77) is $t_1^* \approx 0.6157$ and the first singularity is at $z = it_1^*$. We construct a rectangular contour on the complex plane with the first

singularity inside as in Fig. 21 to evaluate the integral (74), where C is the line segment from $z = -R$ to $z = R$, Γ_1 is the line segment from $z = R$ to $z = R + it_2$, Γ_2 is the line segment from $z = R + it_2$ to $z = -R + it_2$ and Γ_3 is the line segment from $z = -R + it_2$ to $z = -R$. The height of the rectangle is defined by $t_2 = \pi/(2\alpha) > t_1^*$ such that only the first singularity is inside the contour. By the residue theorem and taking the limit $R \rightarrow \infty$,

$$\lim_{R \rightarrow \infty} \int_{C+\Gamma_1+\Gamma_2+\Gamma_3} F(z, \alpha) e^{i\xi z} dz = 2\pi i \cdot \text{residue of } F(z, \alpha) e^{i\xi z} \text{ at } z = it_1^*. \quad (78)$$

Now consider the integrals on Γ_1 , Γ_2 and Γ_3 . First, on Γ_1

$$\begin{aligned} \lim_{R \rightarrow \infty} \left| \int_{\Gamma_1} F(z, \alpha) e^{i\xi z} dz \right| &= \lim_{R \rightarrow \infty} \left| \int_0^{t_2} F(R + it, \alpha) e^{-\xi t + i\xi R} dt \right| \\ &\leq \int_0^{t_2} \lim_{R \rightarrow \infty} |F(R + it, \alpha) e^{-\xi t}| dt \\ &\leq \int_0^{t_2} \lim_{R \rightarrow \infty} \left[\frac{(2|K| + |N_1 - N_2| |z|^2) |\sinh(\alpha z)|}{|\sinh(2\alpha z)| - |z| |\sin 2\alpha|} + \frac{|N_1 - N_2| |\cot \alpha| |z| |\cosh(\alpha z)|}{|\sinh(2\alpha z)| - |z| |\sin 2\alpha|} \right] dt. \end{aligned} \quad (79)$$

We can bound the $|F|$ using following inequalities

$$|\sinh \alpha z| = |\sinh \alpha R \cos \alpha t + i \cosh \alpha R \sin \alpha t| \leq 2 |\cosh \alpha R| = |e^{\alpha R} + e^{-\alpha R}|, \quad (80)$$

$$|\cosh \alpha z| = |\cosh \alpha R \cos \alpha t + i \sinh \alpha R \sin \alpha t| \leq 2 |\cosh \alpha R| = |e^{\alpha R} + e^{-\alpha R}|, \quad (81)$$

$$|z| \leq \sqrt{R^2 + t_2^2}, \quad (82)$$

$$\begin{aligned} |\sinh 2\alpha z| &= |\cosh 2\alpha R \cos 2\alpha t + i \sinh 2\alpha R \sin 2\alpha t| \\ &\geq |\sinh 2\alpha R \cos 2\alpha t + i \sinh 2\alpha R \sin 2\alpha t| \geq |\sinh 2\alpha R|. \end{aligned} \quad (83)$$

Then

$$\begin{aligned} \lim_{R \rightarrow \infty} |F| &\leq \lim_{R \rightarrow \infty} \left[\frac{(2|K| + |N_1 - N_2| (R^2 + t_2^2)) |2 \cosh(\alpha R)|}{|\sinh(2\alpha R)| - \sqrt{R^2 + t_2^2} |\sin 2\alpha|} \right. \\ &\quad \left. + \frac{|N_1 - N_2| |\cot \alpha| \sqrt{R^2 + t_2^2} |2 \cosh(\alpha R)|}{|\sinh(2\alpha R)| - \sqrt{R^2 + t_2^2} |\sin 2\alpha|} \right] = 0. \end{aligned} \quad (84)$$

Thus,

$$\lim_{R \rightarrow \infty} \int_{\Gamma_1} F(z, \alpha) e^{i\xi z} dz = 0. \quad (85)$$

For the same reason,

$$\lim_{R \rightarrow \infty} \int_{\Gamma_3} F(z, \alpha) e^{i\xi z} dz = 0. \quad (86)$$

For the Γ_2 contour

$$\begin{aligned} \lim_{R \rightarrow \infty} \left| \int_{\Gamma_2} F(z, \alpha) e^{i\xi z} dz \right| &\leq \lim_{R \rightarrow \infty} \int_{-R}^R |F(s + it_2, \alpha) e^{-\xi t_2 + i\xi s}| ds \\ &\leq \left[2|K| \left| \int_{-\infty}^{\infty} \frac{\sinh(\alpha(s + it_2))}{\sinh(2\alpha(s + it_2)) + (s + it_2) \sin(2\alpha)} ds \right| \right. \\ &\quad + \left(\left| \int_{-\infty}^{\infty} \frac{(s + it_2)^2 \sinh(\alpha(s + it_2))}{\sinh(2\alpha(s + it_2)) + (s + it_2) \sin(2\alpha)} ds \right| \right. \\ &\quad \left. \left. + \left| \int_{-\infty}^{\infty} \frac{(s + it_2) \cot \alpha \cosh(\alpha(s + it_2))}{\sinh(2\alpha(s + it_2)) + (s + it_2) \sin(2\alpha)} ds \right| \right) \cdot |N_1 - N_2| \right] \times e^{-\xi t_2}. \quad (87) \end{aligned}$$

All three integrals in the square brackets of Eq. (87) are finite, so the bound on the integral on contour Γ_2 is of order $e^{-\xi t_2}$ for $\xi \gg 1$.

Finally, consider the residue from the singularity:

$$\begin{aligned} 2\pi i \cdot \text{residue of } F(z, \alpha) e^{i\xi z} \text{ at } it_1^* &= 2\pi i \lim_{z \rightarrow z_1^*} (z - z_1^*) F(z, \alpha) e^{i\xi z} \\ &= -2\pi e^{-\xi t_1^*} \cdot \frac{2K + (N_1 - N_2)t_1^*(t_1^* - \cot \alpha \coth \alpha t_1^*)}{2\alpha \cos 2\alpha t_1^* + \sin 2\alpha} \times \sin \alpha t_1^* \sim \mathcal{O}(e^{-\xi t_1^*}). \quad (88) \end{aligned}$$

From Eq. (72), $\xi \gg 1$ near the corner. Then the integral on Γ_2 is asymptotically smaller than the residue at $z = it_1^*$ because $e^{-\xi t_2} \ll e^{-\xi t_1^*}$. Thus the dominant asymptotic contribution to the integral is

$$I \sim \frac{1}{2} \text{Re} \{ 2\pi i \cdot \text{residue of } F(z, \alpha) e^{i\xi z} \text{ at } z = it_1^* \}. \quad (89)$$

Using this result in Eq. (72) we obtain

$$\begin{aligned} \sigma_x + \sigma_y &= H(\xi, \alpha) \cdot I = 4(\cosh \xi - \cos \alpha) \sin \alpha \cdot I \\ &\sim -\frac{2K + (N_1 - N_2)t_1^*(t_1^* - \cot \alpha \coth \alpha t_1^*)}{2\alpha \cos 2\alpha t_1^* + \sin 2\alpha} 2\pi \sin \alpha \sin \alpha t_1^* \cdot \left(\frac{2}{\varepsilon} \sin \alpha \right)^{1-t_1^*}, \quad (90) \end{aligned}$$

where t_1^* is the smallest nonzero root of Eq. (77). Recalling that $\varepsilon = \pi/2 - \theta$ is the proximity to the corner, since $t_1^* < 1$, $\sigma_x + \sigma_y$ has an integrable singularity at the corner. Note the exponent $1 - t_1^*$ matches the exponent for the singular solutions for an infinite wedge geometry [29], as Eq. (77) is equivalent to Eq. (29). More generally, for $\pi/2 < \alpha < \pi$ (cases like Fig. 12) there is an integrable singularity with $1 < t_1^* < 2$, and for $0 < \alpha < \pi/2$ (cases like Fig. 8) there is no singularity because $0 < t_1^* < 1$.

Acknowledgements We thank Jeremy Hoskins for a helpful discussion on numerical aspects of this work.

References

1. Boyd JP (2001) Chebyshev and Fourier spectral methods, Dover, New York, pp 19–60

2. Bremer J, Gimbutas Z, Rokhlin V (2010) A nonlinear optimization procedure for generalized Gaussian quadratures. *SIAM J Sci Comput* 32:1761–1788
3. Burton WK, Cabrera N, Frank F (1951) The growth of crystals and the equilibrium structure of their surfaces. *Philos Trans Royal Soc A* 243:299–358
4. Cabrera N (1964) The equilibrium of crystal surfaces. *Surf Sci* 2:320–345
5. Chiu CH (2020) The model of eye-shaped voids: Elasticity solution and its applications in material failures via morphological transformation. *J Mech Phys Solids* 137:103822
6. Clenshaw CW (1955) A note on the summation of Chebyshev series. *Math Comput* 9:118–120
7. Di Carlo A, Gurtin M, Podio-Guidugli P (1992) A regularized equation for anisotropic motion-by-curvature. *SIAM J Appl Math* pp 1111–1119
8. Driscoll TA, Trefethen LN (2002) Schwarz-Christoffel mapping. Cambridge University Press, Cambridge
9. Epperson JF (1987) On the Runge example. *Am Math Mon* 94:329–341
10. Golovin A, Davis S, Nepomnyashchy A (1998) A convective Cahn-Hilliard model for the formation of facets and corners in crystal growth. *Physica D* 122:202–230
11. Golub GH, Welsch JH (1969) Calculation of Gauss quadrature rules. *Math Comput* 23:221–230
12. Gonzalez O, Stuart AM (2008) A first course in continuum mechanics, Cambridge University Press, Cambridge, pp 311–312
13. Gurtin ME (1993) Thermomechanics of evolving phase boundaries in the plane, Oxford University Press, New York, pp 105–110
14. Herring C (1951) Some theorems on the free energies of crystal surfaces. *Phys Rev* 82:87–93
15. Hoskins JG, Rokhlin V, Serkh K (2019) On the numerical solution of elliptic partial differential equations on polygonal domains. *SIAM J Sci Comput* 41:A2552–A2578
16. Knops RJ, Payne LE (1971) Uniqueness theorems in linear elasticity, Springer, New York, pp 61–82
17. Kolossoff G (1914) On some properties of problems in the plane theory of elasticity. *Z Math Physik* 62:384–409
18. Ling CB (1948) The stresses in a plate containing an overlapped circular hole. *J Appl Phys* 19:405–411
19. Mikhlin S (1957) Integral Equations, Pergamon, London, pp 243–272
20. Motok M (1997) Stress concentration on the contour of a plate opening of an arbitrary corner radius of curvature. *Mar Struct* 10:1–12
21. Muskhelishvili NI (1953) Some basic problems of the mathematical theory of elasticity. Noordhoff, Groningen
22. Pan Z, Cheng Y, Liu J (2013) Stress analysis of a finite plate with a rectangular hole subjected to uniaxial tension using modified stress functions. *Int J Mech Sci* 75:265–277
23. Press WH, Teukolsky SA, Vetterling WT, Flannery BP (1992) Numerical recipes in Fortran 77: the art of scientific computing, Cambridge University Press, Cambridge, pp 150–153
24. Savin GN (1970) Stress distribution around holes, NASA, Washington, D.C., pp 60–100
25. Shampine LF (2008) Vectorized adaptive quadrature in MATLAB. *J Comput Appl Math* 211:131–140

26. Siegel M, Miksis M, Voorhees P (2004) Evolution of material voids for highly anisotropic surface energy. *J Mech Phys Solids* 52:1319–1353
27. Soutas-Little RW (2010) *Elasticity*, Dover, New York, pp 155–193
28. Srolovitz D, Davis SH (2001) Do stresses modify wetting angles? *Acta Mater* 49:1005–1007
29. Williams M (1952) Stress singularities resulting from various boundary conditions in angular corners of plates in extension. *J Appl Mech* 19:526–528
30. Wu C (1982) Unconventional internal cracks, part 1: Symmetric variations of a straight crack. *J Appl Mech* pp 62–68